Spectral distribution of local field potential responses to electrical stimulation of the retina

2016 J. Neural Eng. 13 036003

(http://iopscience.iop.org/1741-2552/13/3/036003)

IOP Publishing Journal of Neural Engineering
J. Neural Eng. 13 (2016) 036003 (14pp) doi:10.1088/1741-2560/13/3/036003

Spectral distribution of local field potential responses to electrical stimulation of the retina

Yan T Wong[1,2], Kerry Halupka[1,3,4], Tatiana Kameneva[1], Shaun L Cloherty[1,2,5], David B Grayden[1,4,6], Anthony N Burkitt[1,4], Hamish Meffin[2,5] and Mohit N Shivdasani[4]

[1] NeuroEngineering Laboratory, Electrical and Electronic Engineering, The University of Melbourne, VIC 3010, Australia
[2] National Vision Research Institute, Australian College of Optometry, Carlton, VIC 3053, Australia
[3] National ICT Australia, Victoria Research Lab, The University of Melbourne, VIC 3010, Australia
[4] Bionics Institute, 384-388 Albert St, East Melbourne, VIC 3002, Australia
[5] Australian Research Council Centre of Excellence for Integrative Brain Function, Department of Optometry and Vision Sciences, The University of Melbourne, Melbourne, VIC 3010, Australia
[6] Centre for Neural Engineering, The University of Melbourne, VIC 3010, Australia

E-mail: wong.y@unimelb.edu.au

Received 20 October 2015, revised 7 March 2016
Accepted for publication 9 March 2016
Published 30 March 2016

Abstract

Objective. Different frequency bands of the local field potential (LFP) have been shown to reflect neuronal activity occurring at varying cortical scales. As such, recordings of the LFP may offer a novel way to test the efficacy of neural prostheses and allow improvement of stimulation strategies via neural feedback. Here we use LFP measurements from visual cortex to characterize neural responses to electrical stimulation of the retina. We aim to show that the LFP is a viable signal that contains sufficient information to optimize the performance of sensory neural prostheses. *Approach.* Clinically relevant electrode arrays were implanted in the suprachoroidal space of one eye in four felines. LFPs were simultaneously recorded in response to stimulation of individual electrodes using penetrating microelectrode arrays from the visual cortex. The frequency response of each electrode was extracted using multi-taper spectral analysis and the uniqueness of the responses was determined via a linear decoder. *Main results.* We found that cortical LFPs are reliably modulated by electrical stimulation of the retina and that the responses are spatially localized. We further characterized the spectral distribution of responses, with maximum information being contained in the low and high gamma bands. Finally, we found that LFP responses are unique to a large range of stimulus parameters (~40) with a maximum conveyable information rate of 6.1 bits. *Significance.* These results show that the LFP can be used to validate responses to electrical stimulation of the retina and we provide the first steps towards using these responses to provide more efficacious stimulation strategies.

Keywords: local field potentials, vision prosthesis, retinal prosthesis, decoding

(Some figures may appear in colour only in the online journal)

Introduction

In recent years, there have been many advances toward restoring useful visual perception to people suffering from vision loss. Specifically, human trials involving retinal prostheses that target surviving retinal neurons with electrical stimulation have shown that these devices can aid in rudimentary activities ranging from simple light localization to independent navigation and even reading large font (Fujikado *et al* 2011, Zrenner *et al* 2011, Dorn *et al* 2013, Ayton

et al 2014). Success of these trials has led to the first retinal visual prostheses now being commercially available (Ho *et al* 2015, Stingl *et al* 2015).

While successful human implantations have demonstrated the promise of these devices in providing artificial vision, there are still significant limitations such as low spatial and temporal resolution and challenges in selectively activating specific retinal neurons (Zrenner 2013). Animal studies provide a complimentary path to test novel stimulation methods that may solve some of these issues (Wong *et al* 2009, Dumm *et al* 2014). Specifically, studies that allow recording of neural signals in response to electrical stimulation provide an optimal way to test and fine-tune stimulation parameters (Priori *et al* 2013, Jepson *et al* 2014a, 2014b).

Many studies have focused on measures of spiking activity since it reflects the output of a single neuron or up to tens of neurons. However, the local field potential (LFP) may provide a more suitable signal for the optimization of stimulus parameters. The LFP is defined as the low frequency components (typically < 300 Hz) of neural activity and is thought to be generated by the summation of transmembrane currents (Mitzdorf 1985). The different frequency components of the LFP are also hypothesized to reflect neuronal processes occurring at different cortical scales (Buzsáki *et al* 2012). The LFP is a measure of the population activity across an area of cortex as opposed to the activity of a single neuron and, therefore, is more stable and easier to record (Flint *et al* 2012). As a population metric, the LFP also has the advantage of being less biased by the stochastic nature of sampling individual neuron firing rates (Panzeri *et al* 2007).

Therefore, the LFP has emerged as an important signal for a variety of different neural prostheses such as brain-machine interfaces (Markowitz *et al* 2011, Flint *et al* 2013) and deep brain stimulators (Priori *et al* 2013). In these examples, the LFP has been used either as a primary signal to control a prosthetic device or as a neural feedback signal to fine-tune stimulation parameters.

However, the recording stability may result in a lower spatial resolution of information conveyed, potentially limiting the LFP's usefulness for neural prostheses that require high spatial resolution. From experiments in the visual system, it has been estimated that measures of the LFP integrate activity across an area of ~250 μm from the tip of a microelectrode (Katzner *et al* 2009, Xing *et al* 2009). Whether the LFP can provide neural feedback with such resolution for electrical stimulation from a visual prosthesis is unknown (Waldert *et al* 2009).

Early studies showed that cortical LFPs could be broadly modulated by electrical stimulation of the retina from epi-retinal and sub-retinal implant placements (Schanze *et al* 2002, Eckhorn *et al* 2006). Cottaris and Elfar (2009) then showed that the broadband LFP power could be used to decode electrode configurations and stimulus parameters for stimulation of the retina from the epi-retinal space. The LFP decoder was used to characterize the performance of their epi-retinal approach via an information metric, finding a maximum conveyed information rate of ~4.25 bits with 64 different stimulation parameters.

In this work, we comprehensively investigate the frequency and phase responses of the LFP to electrical stimulation of the retina from the suprachoroidal space (Sakaguchi *et al* 2004, Wong *et al* 2009, Cicione *et al* 2014) and use the LFP to compare the maximum information deliverable by this device to that of other retinal approaches. This is the first study to analyze multi-site LFP responses to suprachoroidal stimulation; our results show that the LFP is highly informative about the stimulation parameters. The study shows also that suprachoroidal stimulation generates discriminable cortical LFP responses with a close correspondence from stimulus to response. Furthermore, all experiments that we present utilize electrode arrays similar to those used in recent human trials by Bionic Vision Australia (Ayton *et al* 2014, Shivdasani *et al* 2014), allowing results to be directly relatable to clinical practice.

Materials and methods

Anesthesia and surgery

Data were collected from four normally sighted adult cats ($n = 4$) implanted with a stimulating electrode array in the suprachoroidal space of a single eye and a recording array in the contralateral visual cortex. All procedures were approved by the Bionics Institute Animal Ethics Committee (formerly the Royal Victorian Eye and Ear Hospital Animal Ethics Committee; Projects 12/255AB and 14/304AB). Each animal was initially anaesthetized with ketamine (20 mg kg^{-1}, intramuscular (i.m.)) and xylazine (2 mg kg^{-1} subcutaneous (s.c.)) and maintained with a continuous intravenous infusion of sodium pentobarbitone (60 mg kg^{-1} h^{-1}). Animals were given daily doses of dexamethasone (0.1 mg kg^{-1} i.m.) to reduce brain swelling and antibiotics (clavulox, 10 mg kg^{-1} s.c.). Pupils were dilated with a topical application of phenylephrine hydrochloride (2.5%) and tropicamide (1%). A continuous infusion of fluid (Hartmann's solution 1.5 mg ml^{-1} h^{-1}) was provided and the respiration rate, end-tidal CO_2, and core body temperate were monitored.

To implant the stimulating electrode array, a full-thickness incision was made through the sclera approximately 5 mm behind the corneal limbus and then a 'pocket' was opened within the suprachoroidal space (Saunders *et al* 2014). The arrays were implanted ~15 mm into the pocket so that the electrode contacts were situated in the area centralis. The stimulating electrode arrays contained 21 circular platinum electrodes each with an exposed diameter of 600 μm and were organized in a staggered 3 × 7 grid, with two large (2 mm diameter) return electrodes on the proximal end of the array. The center-to-center spacing between electrodes was 1 mm, which equates to a visual angle of ~4° (Hubel and Wiesel 1959).

For the recording electrode, a craniotomy was performed over the visual cortex (Tusa *et al* 1978) in the contralateral hemisphere to the eye with the stimulating electrode and the dura mater was removed. To record neural activity, penetrating microelectrode arrays (60 channels, 6 × 10

arrangement, 1 mm length, 400 μm spacing, Blackrock Micro., USA) were implanted into the visual cortex. The location of implantation of the cortical array was optimized with respect to the location of the stimulating array determined using evoked potential recordings from the cortical surface in response to retinal stimulation as described in previous studies (Cicione *et al* 2014, Dumm *et al* 2014). All cortical recordings were referenced to a platinum wire inserted into the temporal muscle.

Electrical stimulation and neural signal recording methods

In all animals, cortical responses to single electrode retinal stimulation were recorded. The stimuli used were single cathodic-leading biphasic current pulses (500 μs per phase, 25 μs interphase gap) on one electrode at a time. In all animals, currents from 0 to 1.5 mA (corresponding to a maximum safe charge density of less than 300 μC cm^{-2} per phase) were tested in 100 μA increments; in one animal (a55) further tests were done in 50 μA increments. Each stimulation amplitude was repeated ten times in random order at a repetition rate of 1 Hz. A subset of electrodes that were not utilized to deliver charge to the retina due to time constraints or technical reasons were removed from further analysis.

Neural signals were recorded at a sampling rate of 30 kHz (Blackrock Micro., USA). To obtain the LFP, the broadband signal (0.1 Hz–7.5 kHz) was low-pass filtered at 400 Hz using a multitaper-spectral technique (Thomson 1982, Mitra and Pesaran 1999) (multitaper projection filter settings; (time duration = 25 ms, frequency bandwidth = 400 Hz, center frequency = 0 Hz)). The LFP signal was then downsampled to 2.5 kHz. The spectrum of the LFP for time steps pre- and post-stimulation were then estimated (MATLAB, MathWorks, USA) with a temporal resolution of 0.8 ms, a frequency resolution of 2.5 Hz, and a 16 ms Hamming window. The time-frequency spectrograms presented were normalized to the average power in each recording channel 0–50 ms before the stimulus onset. For all figures, the mean and standard error of the mean has been shown unless otherwise stated.

To test for significant changes in LFP power in the time-frequency spectrograms, a permutation test was performed comparing the power in each frequency and time period after the stimulus to the power in the 50 ms preceding the stimulus. A minimum of 10 000 permutations were performed for each test. To correct for multiple comparisons, cluster correction to a significance level of $p < 0.05$ was applied to the statistical tests (Maris *et al* 2007). To classify electrodes as exhibiting significant evoked responses, a single Wilcoxon Rank sum test was performed ($p < 0.05$) at ~110 Hz, 13 ms after the stimulus pulse onset (chosen due to the peak in the responses). To analyze how significant responses spread across the cortex with changing stimulus parameters, we calculated a normalized weighted distance measure

$$D = \frac{\sum_i r_i d_i}{\sum_i r_i},$$

where r_i is the magnitude of the response on a given cortical electrode, i, and d_i is the cortical distance in mm from electrode i to the electrode on the array with the maximal response.

To estimate how the spatial spread of responses across the cortical electrodes could correspond to perceived visual experiences, the width of the cortical response was calculated and a cortical magnification factor of 0.3–0.5 mm deg^{-1} was used. This was derived from the cortical recording locations' anatomical maps (Tusa *et al* 1978) and prior studies (Walter *et al* 2005). Significant changes in the phase of the LFP were then tested using a permutation test (10 000 permutations) against the phase in the 50 ms period before the stimulus. Bonferroni correction was used to control for multiple comparisons to a level of $p < 0.05$. Finally, the effect of stimulating electrode location on cortical response shift was examined by first finding the cortical recording channel with the largest response to stimulation at 300 μA. Then, the relative Euclidean distance between the electrodes with maximal response was calculated as a function of the distance between the stimulating electrodes used to generate the response. Here we assumed a cortical magnification factor of 0.3 mm deg^{-1} regardless of eccentricity (Tusa *et al* 1978).

Decoding stimulus features and characterizing with an information metric

To test the uniqueness of the evoked responses, the LFP was decoded to predict the electrical stimulation parameters used to generate the responses (stimulating electrode identity and current level). The decoding algorithm was comprised of three stages: preprocessing, extraction of features, and classification (Markowitz *et al* 2011). In the preprocessing stage, for each trial and each recording channel, a time window of LFP data was extracted and transformed into the frequency domain (described above). The resulting frequency domain data across all the recording channels was collapsed to form a single vector of a length determined by the number of recording channels (60) multiplied by the number of frequency bins (160 for all LFP frequency bands, 1–400 Hz). Essentially, frequency bands and recording channel identities were removed and treated independently with one vector representing the response to each stimulation trial and time window. This was repeated for each trial and for time windows before and after the stimulus.

Decoding was performed at individual time points that varied from 20 ms before stimulation to 100 ms after. The decoding performance of four different spectral bands (1–30 Hz, 40–100 Hz, 101–300 Hz, and 1–400 Hz) corresponding roughly to beta, low-gamma, high-gamma, and all frequency bands was also tested. Frequency steps were identical for all groupings. To do this, the signal in each spectral band was estimated before performing the previously described preprocessing methods.

Next, to reduce the dimensionality of these vectors, an orthogonal transformation (principle component analysis, PCA) was used to generate a set of uncorrelated features. The

150 features that captured the most variance of the original space were used by the decoder to predict the stimulation parameters. This number was chosen through an iterative process, where the number of features was increased and the decoding performance of a random sample of data examined. With increasing features, the decoding performance plateaued and a point beyond the plateau was chosen. This was done through a linear discriminant analysis, which effectively clustered the feature responses to different stimulation parameters (electrode number and stimulation level) (Duda *et al* 2012). As an example, when decoding responses from two different stimulus parameters (or classes; $U_{\text{trial}} \in \{0,\ 1\}$), the analysis fitted a linear, discriminant function, $f(x)$, that best separated the transformed neural activity in response to the two classes. The discriminant function is given by

$$f(x) = w^T x + a,$$
$$w = C^{-1}(\mu_2 - \mu_1),$$
$$a = -w^T \mu,$$

where x is the feature vector of the PCA transformed, frequency domain neural responses. The w parameters for the above equation were fit using training data that included an equal number of responses from both classes, with μ_1 and μ_2 representing the means of each class, μ the mean of both classes, and C the pooled covariance of both classes.

To decode class labels for a separate test set, $f(x)$ is calculated for each trial of data in the set and assigned to class 0 if $f(x) < 0$ or to, class 1 if $f(x) \geqslant 0$. To extend this to decoding more than two stimulus parameters, a one-versus all classification approach was taken, where a binary decoder was created for all class pairs. Class labels were then assigned by

$$k = \underset{i}{\text{argmax}} \sum_j f_{ij}(x),$$

where $f_{ij}(x)$ denotes the decoder for classes i and j, and k the classified class label. The decoding estimates from the above method were bootstrapped using a leave-one-out cross validation method.

Finally, to test differences in the information contained in the magnitude and phase of the LFP, the decoding was performed by calculating and including either the phase (represented as a number in $[0, 2\pi)$), magnitude, or both phase and magnitude in the preprocessing stage. For this comparison, all other stages of decoding remained the same. In this manuscript, the mean correct performance of decoding averaged across all decoded parameters is shown, as well as confusion matrices that detail how each stimulation parameter was predicted. Confusion matrices are plotted for data taken from the first positive peak after the stimulation pulse.

To characterize the performance of suprachoroidal stimulation in generating uniquely discriminable responses and to compare this to previously published results from other stimulation locations such as the epi-retinal approach, a mutual information metric described by Cottaris and Elfar (2009) was calculated. Specifically, we calculated the mutual information, $I(\tilde{S};\ S)$, between the decoded stimulation parameters, $\tilde{S}$, and the actual stimulation parameters, S. This is given by

$$I(\tilde{S};\ S) = \sum_{u=1}^{N}\sum_{v=1}^{N} P_{\tilde{S}S}(u,\ v) \log \frac{P_{\tilde{S}S}(u,\ v)}{P_{\tilde{S}}(u) P_S(v)},$$

where $P_{\tilde{S}}(u)$ and $P_S(v)$ are the marginal probability distributions with

$$P_{\tilde{S}}(u) = \sum_{v=1}^{N} P_{\tilde{S}S}(u,\ v)$$

and

$$P_S(v) = \sum_{u=1}^{N} P_{\tilde{S}S}(u,\ v) = \frac{1}{N}$$

as each stimulation parameter was presented an equal number of times. Here, u represents the individual stimulus parameters presented (from 1 to N), and v represents the decoded stimulus parameter identities from the classifier described in the earlier section. Information metrics were also corrected for bias using a Miller-Madow correction where the bias, B, is given by

$$B = \frac{\hat{m} - 1}{2n},$$

where $\hat{m}$ is the number of bins with non-zero probabilities and n is the number of samples (Miller 1955, Panzeri *et al* 2007). To measure how well each individual stimulus parameter was decoded from the rest, a sensitivity index, d', was calculated for each stimulus parameter (Cottaris and Elfar 2009):

$$d' = Z(\text{hit rate}) - Z(\text{false alarm rate}),$$

where Z represents the z-score of each probability of detection. The 'hit rate' is the probability that a given stimulus parameter (e.g. current level 1 from electrode 1) is correctly identified (as current level 1 from electrode 1), whereas the 'false alarm rate' is the probability of other stimulus parameters (stimuli 2 to N) being incorrectly classified as stimulus 1.

Finally, to calculate how mutual information varied with different set sizes (the number of available stimulation parameters), d' was used to iteratively remove the worst decoded stimulus parameter. In this analysis, all stimulus parameters were decoded at the first iteration. For every subsequent iteration, the stimulus parameter with the lowest d', which reflected the least well decoded parameter, was removed from the set and the decoder was re-run. This was performed until only a single stimulus parameter was left. To test the robustness of this method, the same analysis was repeated but, instead of removing the stimulus parameter with the lowest d', a stimulus parameter in the lowest ten was randomly chosen and removed from subsequent iterations. For the time stepped decoding analysis, three currents were decoded on each electrode (100, 500, and 1000 μA) chosen from thresholds and dynamic ranges previously reported (Cicione *et al* 2014, Dumm *et al* 2014). For the mutual information analysis, currents ranging over 0–1.5 mA in 100 μA steps for three animals and in 50 μA steps for one animal were decoded.

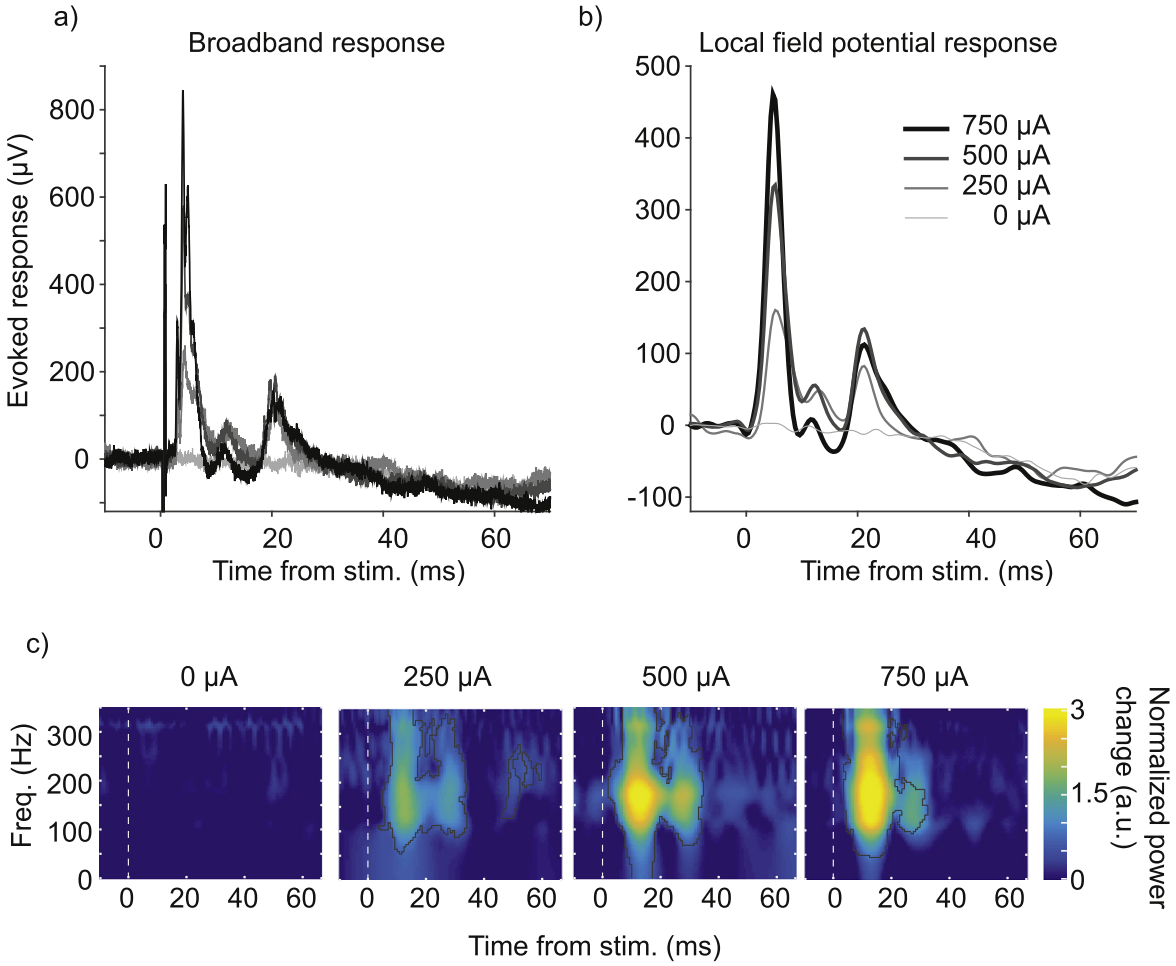

Figure 1. Example of an averaged (a) broadband (0.01–7.5 kHz) and (b) local field potential (0.1–400 Hz) response to suprachoroidal electrical stimulation of the retina at different current levels. Each stimulus was delivered with a biphasic pulse with a phase duration of 500 μs. Responses increased in amplitude with increasing current levels. The stimulus artifact contamination (at 0 ms) in the broadband average was not dominant after filtering to generate the local field potential average. (c) Time-frequency spectrograms of the local field potential responses shown in panel (b). Spectrograms were normalized to the baseline power 50 ms pre-stimulus and significant changes in power from baseline are indicated with black lines.

Results

LFPs are modulated by electrical stimulation

There was a robust and immediate neural response to electrical stimulation of the retina delivered from the suprachoroidal space. The broadband signals showed an initial peak within 10 ms of the stimulus and a secondary peak after 20 ms. The amplitude of the initial peak increased in magnitude as the current level was increased. The broadband response recorded on a single recording channel following electrical stimulation of a single stimulating electrode in the suprachoroidal space is shown in figure 1(a). The peaked response and ordering seen in the broadband signal remained after filtering to obtain the LFP (figure 1(b)). The large stimulus artifact, which is prominent in the broadband response (peak at 0 ms), was suppressed in the LFP averages, as would be expected for a biphasic pulse with phase durations of 500 μs.

Time-frequency decompositions of the LFP signals were calculated from these responses to allow the information carried in each frequency band and the time evolution of this information to be compared across recording channels and stimulating electrodes. The resulting spectrograms (figure 1(c)) showed that a significant double-peaked response occurred in the range 100–200 Hz (black lines show regions with significant changes from baseline period power, $p < 0.05$ cluster-correct permutation test). With increasing current levels, the power within this band increased.

To examine whether these effects existed across the population of responses, all combinations of recording channels and stimulating electrodes were tested for a significant response at four different current levels (0, 200, 500, and 700 μA). Figure 2(a) illustrates the population response using the same conventions as in figure 1(c). In total, 4380 stimulating/recording pairs were tested, with the number of significant pairings stated on the top right of each panel. A significant increase in power between 100 and 200 Hz was again prominent in the population average with multiple peaks visible. With increasing current levels, power in this band increased, the number of recording channels showing a

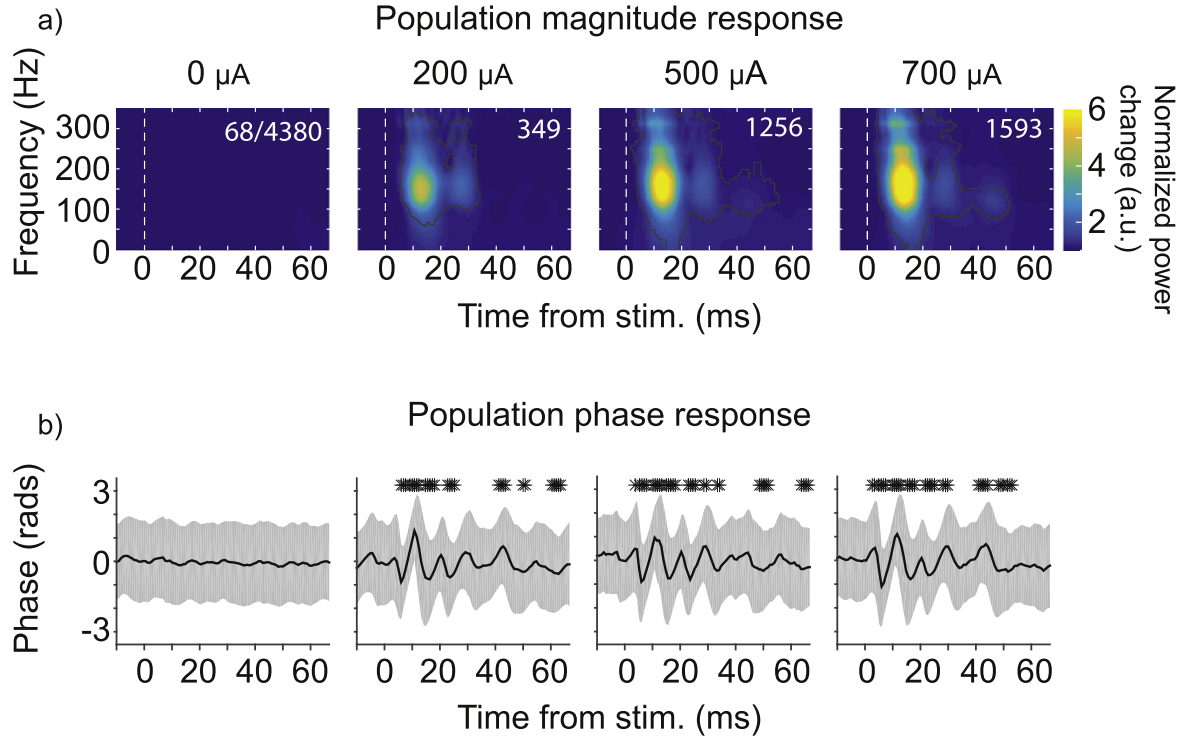

Figure 2. (a) Population average responses (magnitude of the spectrum of the LFP) across all animals to four current levels. Only recording channels that exhibited a significant response from baseline were averaged. The number of significant recording channel-stimulating electrode combinations for each stimulation level is shown in the top right hand corner of each spectrogram. A significant change in power of the LFP can be seen shortly after the stimulus onset (highlighted with a black line $p < 0.05$ cluster-corrected rank sum test). At 0 μA current, channels with a non-significant response are shown. (b) The population average of the instantaneous phase (at ~110 Hz) of the LFP in response to the same stimulation parameters. Significant changes in the phase from baseline are indicated with stars ($p < 0.05$, Bonferroni corrected permutation test). The mean $\pm$ s.t.d. are shown.

significant response increased, and a third peak in the response between 40 and 50 ms became significant (stimulus current > 500 μA).

In addition to the magnitude of the LFP response, the instantaneous phase was also significantly modulated by electrical stimulation. Figure 2(b) shows the corresponding population average phase changes at ~110 Hz to the four different levels of stimulation. Significant changes in the phase from baseline are indicated by asterisks above each plot. These results show that the LFP was modulated reliably and broadly by electrical stimulation in the suprachoroidal space.

LFP responses are spatially localized

The previous analyses examined responses on individual electrodes; however, an important aspect for visual prostheses is the relationship between stimulus parameters and the spatial extent of the evoked response. As expected for increasing stimulating current levels, the spread of the response increased across the recording channels. An example of this is illustrated in figure 3, where the response across all the cortical recording channels (60) to two different current levels delivered from a single stimulating electrode is shown. The response to 100 μA stimulation (figure 3(a)) was more focused spatially than the response to 250 μA stimulation (figure 3(b)). The response was also lower in magnitude on individual electrodes that did respond. For these examples, the response at the peak of the spectrum 240 Hz, ~15 ms post stimulus is plotted in figures 3(c) and (d).

To quantify these trends across electrodes and animals, the number of recording channels that responded significantly at different time points, different frequencies, and to different current levels delivered from the stimulating electrodes was characterized. As expected, the number of significant recording channels increased as a function of stimulus current with an average of 4.4 ± 1.4 electrodes (mean $\pm$ s.e.) showing a significant response at 200 μA (corresponding to a visual angle of 1.6°–2.7°), eventually plateauing at ~28 electrodes at 1.2 mA (figure 3(e)). Further increases in current did not lead to a further increase in the number of significantly activated electrodes (1.2 mA: 28.4 ± 2.4 electrodes, 1.5 mA: 28.3 ± 2.4, $p = 0.96$; rank sum test). Tests for significance were performed at 240 Hz, ~15 ms after the stimulus onset at the peak of the average response.

When examining the spread of activity as a function of time (figure 3(f)), two clear peaks were present with a third smaller but significant peak at 40 ms ($p = 10$ e^{-5}; signed-rank test). For figure 3(f), tests for significance were performed at 240 Hz for a 1 mA stimulus. Finally, when looking at how activity spread as a function of the frequency band of interest, the number of significant channels increases to a peak at 300 Hz (figure 3(g)). Tests for significance were

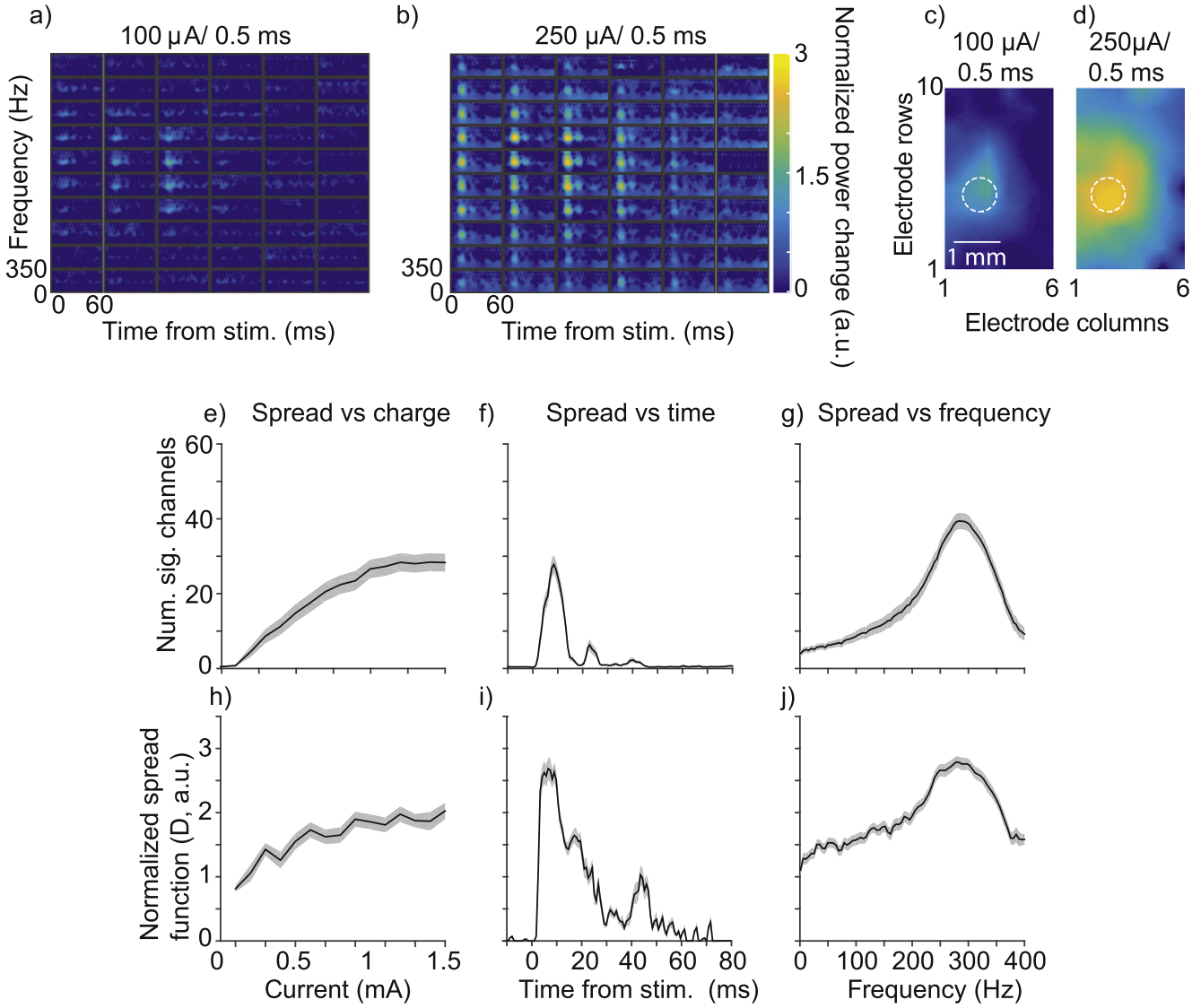

Figure 3. (a) Example spectrograms across the 60 recording channels in response to a 100 μA stimulus from one animal. Each individual panel shows the time-frequency response on one recording channel. The panels are spatially arranged in the same organization as the recording array (i.e. 6 $\times$ 10 grid). In this example, a small localized response can be seen in the middle left of the array. (b) With increasing current, responses increased in magnitude and spread across the array. (c), (d) The response across the cortex for the examples presented in (a) and (b). The magnitude of the response at 240 Hz and ~15 ms post stimulus across the 6 $\times$ 10 array are shown. Data has been interpolated. Superimposed in white, is the idealized approximate response spread for a retinal electrode diameter of 600 μm and a cortical magnification of 0.3 mm deg^{-1}. The cortical spread was summarized by (e) examining the number of channels that significantly responded to a stimulus as a function of the charge injected, (f) the time point at which the significance test was performed, and (g) the frequency at which the significance test was performed. The size of the spread of the response was also characterized for (h) increasing currents, (i) different time points, and (j) different frequencies. For (e)–(j) the mean $\pm$ s.e.m. are shown.

performed ~15 ms after a 1 mA stimulus corresponding to the first peak shown in figure 3(f). When the extent of the spread of activity was analyzed using a normalized weighted distance metric, D, the same trend in results as above emerged (figures 3(h)–(j)). The only major difference occurred 40 ms post stimulus with the spatial spread of the response increasing markedly even though the number of significant channels only changed by a few electrodes (figures 3(f) versus (i)).

Finally, we analyzed how the locations of the cortical responses shifted depending on the locations of the stimulating electrodes. Figure 4 presents the average shift in the location of the maximum response as a function of the shift in stimulus location for pairs of retinal electrodes (n = 505). The location of cortical responses shifted when the retinal stimulus location shifted; however, the degree of displacement was much less than expected from the known retinotopic mapping. This shift also plateaus with larger displacements of the stimulus location. Regardless, these results show that the LFP can be a reliable signal to test for the spread of activity in the visual cortex and that the spread and location of activity is dependent on the amplitude of stimulation, the time period after the stimulus, and the frequency band that is tested.

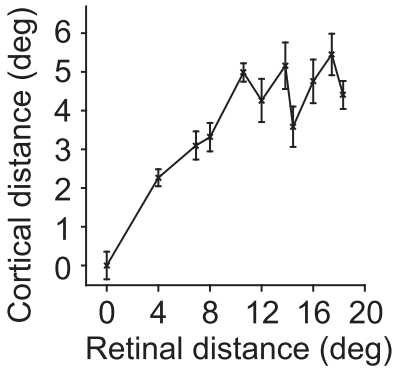

Figure 4. The change in the location of the maximal cortical response as a function of the change in the location of the stimulation site on the retina. Cortical distance has been converted to visual angle using a spatial mapping of 0.3 mm deg^{-1}. The mean and s.e.m. are shown.

LFP responses are unique to different stimuli

While reliably eliciting percepts is important for a visual prosthesis, the efficacy of the implant is highly dependent on the ability to generate a large set of distinguishable percepts. Neural responses to electrical stimulation that are distinguishable from each other would indicate that the resultant percepts may be unique and differentiated from each other. As such, a linear classifier was implemented to decode stimulus parameters from the LFP signals to test the ability to discriminate between the elicited neural responses. For this analysis, the LFP cortical responses from all recording channels to three stimulus amplitudes (100, 500, and 1000 μA, chosen to correspond to three clinically relevant current levels, Shivdasani *et al* 2014) delivered via each of 19 stimulating electrodes was decoded (two electrodes were removed due to insufficient responses). The decoding was performed using all LFP frequencies (1–400 Hz) initially on a single time window of data. This window was then advanced one time-step at a time and the analysis repeated.

The LFP was found to be highly informative, with a peak decoder performance of ~75% in a single subject (figure 5(a)). This suggests that the LFP response is stable across trials and informative of the majority of stimulus configurations (i.e. $19 \times 3 = 57$ stimulating electrodes and current level combinations). However, it is evident from figure 5(a) that the decoder performance exhibited a strong temporal effect. Decoding performance shared similar features to the multipeaked responses seen in the spectrograms, with two large prominent peaks. However, this feature was not present in the population decoding performance (figure 5(b)), which exhibited a single peak in the decoding performance.

The decoding performance of individual stimulus parameters was further broken up to show where the classification confusions lie. Data from the first peak in figure 5(a) were used to generate the confusion matrix shown in figure 5(c). The axes are grouped and sorted according to stimulating electrode so that the first three small squares represented current levels 100 μA, 500 μA, and 1000 μA, respectively, on the stimulating electrode 1, the next three squares represented the same currents on stimulating electrode 2, and so on. From this, the majority of stimulus parameters were decoded with a success rate greater than 85% and most confusions occur for the lower current stimuli (100 μA). This may be due to the current levels on these electrodes being subthreshold to generate a response and hence the resulting neural activity for currents below this level being identical.

To better analyze how the LFP differed in response to the stimulation parameters, the full set of stimuli (31 current levels, 19 electrodes) were decoded and confusion matrices were generated that collapsed stimulus labels across either the stimulating electrode (figure 5(d)) or the current level (figure 5(e)). This analysis revealed that the stimulating electrode identity was encoded in the LFP with high fidelity and that all could be decoded significantly above chance ($p < 0.05$; binomial test). Interestingly, when comparing how well current levels could be decoded from the neural responses, a pattern emerged where currents above a certain level were more confused (bottom right of figure 5(e)) compared to the middle and low ranges of currents. This result is consistent with the plateauing of the spatial spread of response previously presented in figures 3(e) and (h).

LFP information is frequency dependent

Since previous results showed that the spread of activity across the cortical recording array was frequency dependent (figure 3(g)), the decoding performances of band-limited neural signals were next compared. Three frequency bands of interest were chosen: beta (1–30 Hz), low gamma (40–100 Hz), and high gamma (101–300 Hz). Figures 6(a) and (b) present the results from a single animal and for the population average, respectively. Beta band activity was consistently the least informative frequency band, with low and high gamma bands having equal decoding performance during the first peak. In the example shown in figure 6(a), information in the low gamma band was more informative than the high gamma band in the second peak ($p = 0.001$; Rank sum test at ~29 ms after stimulus), with this effect being smaller but still significant across the population average ($p = 0.011$; rank sum test).

In order to test whether the temporal information in the LFP was consistent, or whether the first and second peaks in the response conveyed different information about the stimulus, the decoder was re-run using all LFP frequencies (1–400 Hz) in the data from either the first peak alone or from both the first and second peaks. Information contained in the peaks were found to be redundant with the decoding performance of both decoders is statistically indistinguishable (1st peak: $57.4 \pm 4.2\%$, 1st and 2nd peaks: $56.3 \pm 4.5\%$, $p = 0.74$; rank sum test).

LFP phase provides an alternate source of information

The phase of the LFP was shown to be significantly modulated (figure 2(c)) by electrical stimulation, but it is unknown whether these changes are informative about the stimulation

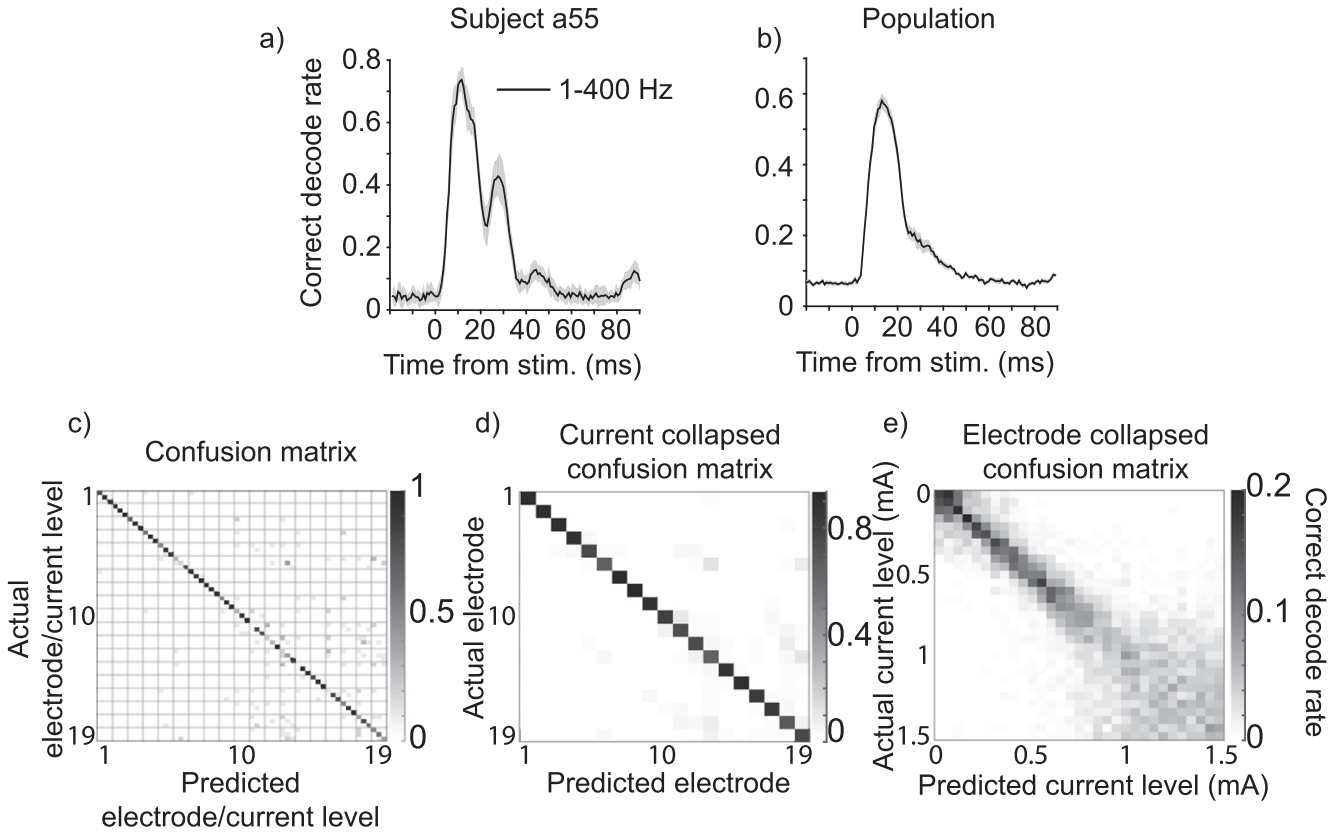

Figure 5. (a) Example from one animal showing the probability of correctly decoding the stimulation parameters (electrode identity and current level) at different time points before and after the stimulus pulse. Shortly after the stimulus was delivered, the decoding performance increased significantly. The mean ± s.e.m. are shown. (b) Population average decoding performance. (c) A confusion matrix for the example in (a), showing the joint distribution of the predicted and observed stimulation parameters. Gray lines indicate the groupings of currents delivered from a single stimulating electrode. The 19 gray lines indicate groupings of three current levels tested for each prediction. (d) A confusion matrix showing the decoding performance for the example in (a) collapsed across electrode identities (decoding electrode identities but not current levels). (e) A confusion matrix showing the decoding performance for the example in (a) collapsed across current levels (decoding current levels but not electrode identities).

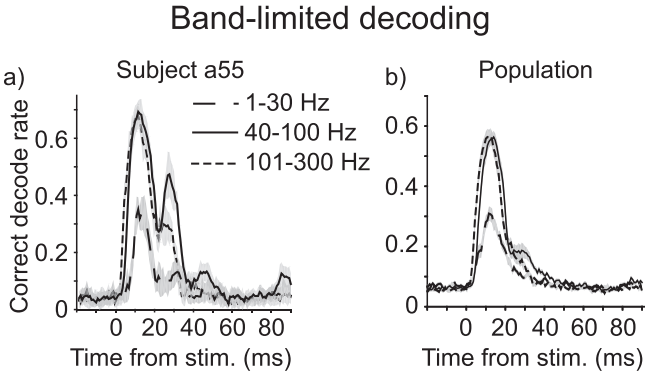

Figure 6. (a) Frequency-band limited decoding performance of the stimulus parameters for a single animal. The mean ± s.e.m. are shown. (b) Population decoding performance for the same band-limited frequency inputs.

parameters. To test this, the phase response alone was used to decode the stimulation parameters. This was done with all the frequencies of the LFP (1–400 Hz) and in the three bands previously identified. The phase of the LFP was found to be broadly informative (figures 7(a) and (b)) with the beta band phases again exhibiting the lowest decoding performance similar to the results found when decoding with magnitude. Interestingly, contrary to what we found when using the magnitude alone, decoding performance of the high gamma phases was better than the low gamma phases for the period between 10 and 15 ms after stimulus onset ($p < 10\,e^{-9}$; rank sum test). Decoding of all frequency bands was also lower for the phases compared to the performance when decoding with magnitude.

Finally, both signals (amplitude and phase) were used simultaneously to decode the stimulus parameters to examine whether the information in the phase was independent of the amplitude of the LFP. The information in the combined LFP phase and amplitude was redundant with no significant differences (all points $p > 0.05$; rank sum test) in the combined decoding performance of the phase and magnitude decoder and the magnitude-alone decoder sessions (figures 7(c) and (d) versus figures 6(a) and (b)).

Calculating the maximum information conveyed by suprachoroidal stimulation

In order to compare the results of suprachoroidal stimulation to other previously published stimulation approaches, the

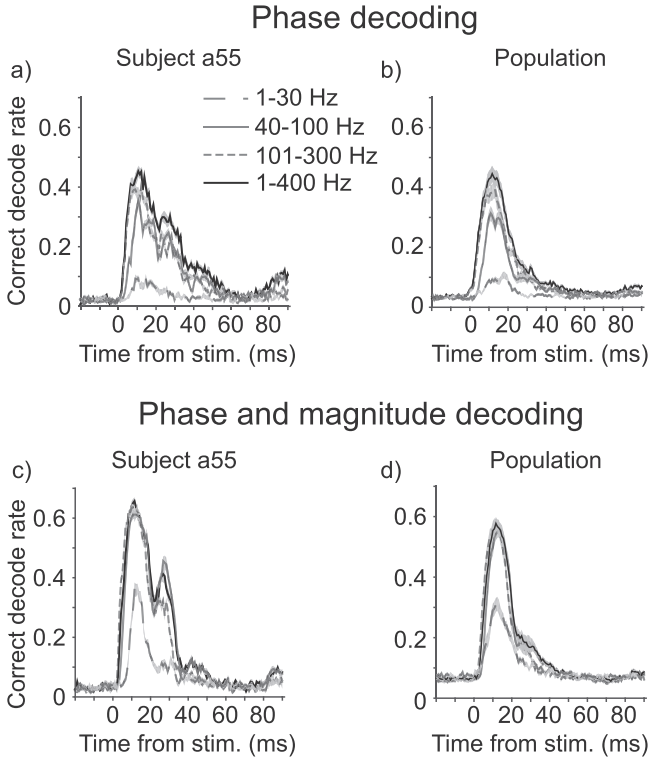

Figure 7. Decoding performance of the phase of the LFP as a function of time. (a) Example from one animal using data from all frequencies as well as when the data were separated according to the different frequency bands. The mean ± s.e.m. are shown. (b) Similar to panel (a), but for the population average data. (c) Decoding performance of the combined phase and magnitude of the LFP in one animal, and (d) for the population average.

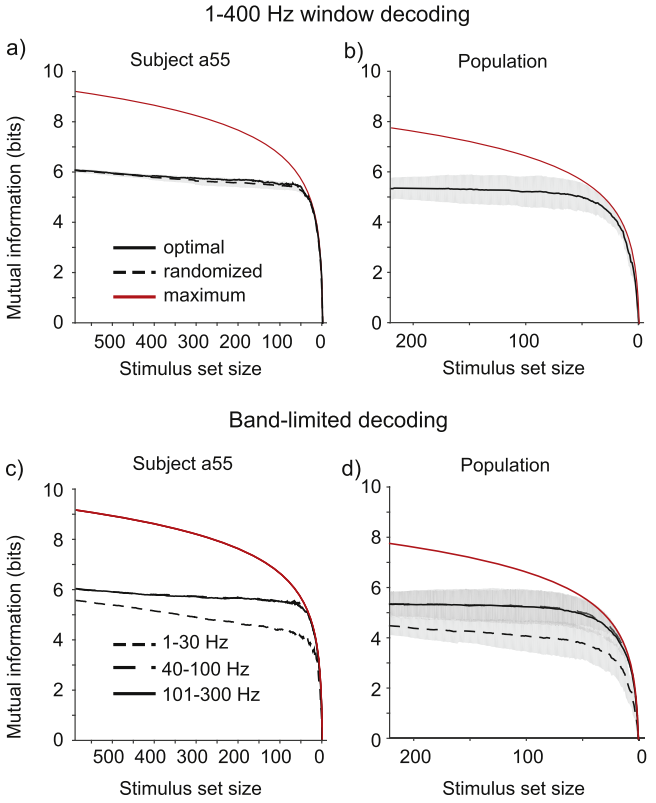

Figure 8. Mutual information as a function of stimulus parameter set size. (a) Mutual information (black lines) for a single animal when the 'optimal' and 'pseudo-random' removal of the least informative stimulus parameters is used. The red lines show the theoretical maximum amount of information that can be conveyed with each stimulus set size. (b) Population average mutual information. For (a) and (b), all frequency bands of the LFP were used. Mutual information of the three frequency bands of interest (c) for the single animal example (d) and for the population average. Mutual information for low gamma and high gamma results are overlapping for panels (c) and (d). The mean ± std are shown.

decoding performance of each session was converted into a standard information metric. This metric was calculated for varying stimulus set sizes. For each session, all stimulus parameter combinations (electrode number and stimulus amplitude, 31 current levels in subject a55, and 16 current levels for all other subjects) were decoded from the magnitude of the LFP, the least informative response was removed (see methods for more details), and the new set of stimulus parameters were decoded. This was repeated until only one stimulus parameter remained.

Figures 8(a) and (b) present the mutual information conveyed by the suprachoroidal prostheses (black lines) with the theoretical maximum information shown in red. For this data, the mean and standard deviation across the animals is shown. For the single subject example (figure 8(a)), there were approximately 50 highly informative stimulus parameters after which the information content conveyed by more stimulus parameters increased slowly. When all 589 stimulus parameters were included from this experiment, the maximum information delivered was 6.08 bits. To ensure that the method of removing the least informative session was accurate, a randomized removal method was also tested with the information conveyed in these sessions being only slightly less, but not significantly lower (all points $p > 0.05$ rank sum test), than that with the optimal method (figure 8(a)). A smaller set of informative stimulus parameters (~40) was also found in the population average analysis (figure 8(b)). At a set size of 221 stimulus parameters, there was a maximum information of 5.4 ± 0.47 bits (mean ± std). For smaller set sizes of 64 stimulus parameters, the total information was 5.14 ± 0.6 bits. These analyses were performed at the time point of maximum decoding performance.

The mutual information metric was also used to compare the differences in information being conveyed in each frequency band. Figures 8(c) and (d) present the single animal and population results, respectively. As previously shown, the high and low gamma band contained statistically identical ($p > 0.05$; rank sum test) information, whereas the beta band was the least informative. This effect remained for decreasing set sizes of the stimulation parameters.

Discussion

The main aim of this work was to examine the properties of the LFP response that can be used to test the effectiveness of neural prostheses. We found that the LFP was highly

informative about the stimulus parameters used to evoke responses and that responses were distinguishable and reproducible to a wide range of stimulus parameters (~40). We also found that the electrically evoked LFP response was multi-peaked, with the first peak the most informative in the low and high gamma frequency bands and that the magnitude of the response was the most informative. When examining the evoked responses with an information metric, we also found that suprachoroidal stimulation was able to provide similar if not more distinguishable responses than certain epi-retinal devices (6.1 bits from a total stimulus set size of 589). These results provide strong evidence that time-frequency decompositions of the LFP can be used to provide feedback in designing new stimulus paradigms and that the stimulation from the suprachoroidal space is effective in generating distinguishable cortical responses.

Neural feedback and the LFP

In a clinical setting, recording of the LFP during electrical stimulation would allow dynamic adjustment of stimulation parameters based on inferring the perceived phosphenes. Ideally, these stimulation parameters would be continuously altered until the responses more closely mimic those elicited by natural light stimulation. Adjustment of stimulation parameters (fitting) has been shown to be a necessary strategy for maximizing auditory perception in cochlear implants (Wilson and Dorman 2008). In cochlear implants, stimulation parameters are fine-tuned for each electrode in response to subject feedback. For a device such as a visual prosthesis, due to a need for substantially larger numbers of stimulating electrodes, tuning of parameters based on overt subject responses will not be clinically feasible. Using a stable, reliable, and easily recorded signal such as the LFP may provide the feedback necessary to adjust stimulation parameters dynamically and on-line (Flint *et al* 2012, 2013), circumventing this issue.

There still remains significant difficulty in defining an objective function that will maximize the usability of a vision prosthesis for a patient. In particular, there is no clear way to optimize cortical responses to the many complex natural scenes that are experienced daily (Kayser *et al* 2003, Weliky *et al* 2003). However, a simple objective function that aims to reduce the cortical spread of responses may provide significant improvements in vision to patients by generating more punctate phosphenes (Wong *et al* 2009).

Another drawback of using a neural signal to provide feedback is, of course, the necessity to implant additional electrodes in the patient. For this reason, the LFP is a particularly attractive choice compared to the use of spiking activity because it can be recorded with less invasive electrodes, such as micro-ECoG or EEG, whereas spiking activity must be recorded with a penetrating electrode and would be less stable over the long periods of time that would be required of a prosthesis. Work in the field of brain-machine interfaces in animals has shown that ECoG recordings can offer decoding performance as good as penetrative LFP recordings (Chao *et al* 2010), with some success in translating this to humans (Wolpaw *et al* 2002, Leuthardt *et al* 2004). However, there have also been results to the contrary where from a simple information viewpoint, penetrating the cortex significantly increases decoding performance (Markowitz *et al* 2011). This decrease in available information may reduce the clinical viability of using dynamic feedback to improve the efficacy of visual prostheses.

Cortical evoked responses

The responses recorded from the visual cortex, evoked by suprachoroidal stimulation in this study were similar in shape and timing to those previously reported for epi-retinal and sub-retinal stimulation (Eckhorn *et al* 2006, Cottaris and Elfar 2009, Wong *et al* 2009). Consistent with these studies, the peak-to-peak magnitude of the broadband response and the spread of the response across the visual cortex increased with increasing stimulus charge delivered. The extent of this spatial spread of activity was found to plateau, which indicates a maximum level of cortical activation. Interestingly, at the lower end of the stimulus levels, we found that a 200 μA stimulus on average activated four cortical recording channels (figure 3(e)). We estimate that this corresponds to an evoked response spanning a visual angle of 1.6°–2.7°. This would be similar to phosphene sizes generated in human trials for suprachoroidal stimulation. Patients have reported experiencing phosphenes similar in size to a 'dime' or 'quarter' (1.7°–2.2°) at an arm's length (Fujikado *et al* 2007). This is, however, larger than the size of phosphenes reported for epi-retinal and sub-retinal stimulation, which typically range from 0.1° to 2° (Humayun *et al* 2003, Wilke *et al* 2011, Zrenner *et al* 2011). The most likely explanation for the increased phosphene sizes is the current spread resulting from increased distance of the stimulating electrodes from the retinal ganglion cells and the need to stimulate through the choroid.

We also find that the shift in the location of the cortical response is less than expected from the known retinotopic mapping. This may be due to two different reasons. The first is the limited cortical coverage provided by the recording array and the relatively large coverage of the stimulating array. With a width of 4 mm, the recording array is unable to record from all corresponding locations of the retina being stimulated. If this were the case, responses to stimulation of distant, more peripheral locations of the retina would result in measured cortical responses that were centered off the array, on the edge of the array, or deep within the cortical sulci. This is the result that we see (figure 4), with the displacement of the cortical response plateauing. This would also be consistent with the variable decoding results across electrodes (figure 5(c)), with electrodes with poor performance, particularly those that were located more peripherally, perhaps generating responses not centered or as well covered by the recording electrode. The second possibility is that stimulation of the retina is not occurring directly under the electrode and is instead being shunted across the retinal tissue. If this is the case, all electrodes should be affected equally; however, our results show a clear plateauing only for distant locations. Further experiments with greater coverage of the cortex with

either more arrays or higher coverage surface electrodes would be required to answer this question.

Frequency dependence of responses

The spatial spread of the LFP response was heavily dependent on the frequency band analyzed. We found that increasing charge injection strongly modulated the activity in the 100–200 Hz (high gamma) frequency band (figure 3(g)). There is growing evidence that the LFP may reflect neuronal processes occurring at varying cortical scales. Specifically, it has been hypothesized that different frequency bands of the LFP reflect specific neuronal processes (Siegel *et al* 2012). Relevant to the work in this study, the low frequency beta band activity (1–20 Hz) is posited to reflect distributed processing that occurs across large networks of neurons (Fries 2005, Donner and Siegel 2011). This is in contrast to low gamma (30–100 Hz) and high gamma (100–200 Hz) bands, which reflect local computations and processing (Schomburg *et al* 2012, Buzsáki and Schomburg 2015), with the high gamma band activity being more closely related to single unit spiking (Ray and Maunsell 2011).

Therefore, we posit that the electrical stimulation generates localized responses in the activity of primary visual cortex. However, we find that the spread of activity across the cortex is greatest in the high gamma band, and perhaps due to this spreading of activity, the information about the stimulus parameters is significantly greater in the low gamma band during the second peak of the response (figures 6(a) and (b)). While this effect is small, it is nonetheless significant and may indicate a different mechanism in the activity present in the second peak.

Finally, to examine the LFP responses comprehensively, we also analyzed the information conveyed in the phase of the LFP (figures 7(a) and (b)). While the phase was informative, it was significantly less so than the magnitude of the LFP and did not contain any new information as revealed by the combined phase-magnitude decoding analysis. The phase of the LFP has been previously reported to increase the information conveyed with spiking information in the visual system (Gray *et al* 1989, Vinck *et al* 2010). Future work to investigating the link between activity in these frequency bands and perceived phosphenes may allow for targeted activation of the LFP in specific frequency bands that is coherent with spiking activity (Kayser *et al* 2009).

Time dependent information changes

The latency of the first peak of the responses (10–15 ms, figure 1(a)) to electrical stimulation showed a similar timing to that reported by other groups (epi-retinal: 10–20 ms Eckhorn *et al* 2006, suprachoroidal: 10–16 ms Nakauchi *et al* 2005, Wong *et al* 2009). This latency is faster than that reported for visual stimulation (>20 ms), which suggests that the photoreceptors have been bypassed and the ganglion cells in the retina were directly activated. In these recordings, we also saw a significant second peak with a latency of 20–30 ms. This secondary peak may arise from secondary indirect activation of the photoreceptors or other retinal neurons, activity mediated by bipolar neurons, or more complex cortico-cortico interactions. From the decoding analysis, we found that the information contained in the second peak was significantly less than that in the first peak and that there was little new information in the second peak (figure 5). Furthermore, information in the second peak was strongest in the low gamma band, which is less a reflection of spiking activity than the high gamma band (figure 6(b)). This further alludes to the possibility that the second peak in the LFP activity arose from cortico-cortico interactions as opposed to secondary activation from the retina.

Information metric comparators

The information metric allowed the results from this study to be compared to other anatomical locations for a retinal prosthesis. We found that the performance of suprachoroidal stimulation in providing distinguishable cortical responses was greater than the 25 channel epi-retinal device reported by Cottaris and Elfar (2009). They reported an information rate of ~4.25 bits with 64 stimulus parameters whereas we found an average information rate of 5.1 bits for the same number of stimulus parameters (figure 8(b)). We also reported a maximum information rate of 6.1 bits for the full stimulus set size (figure 8(a)).

By analyzing the confusion matrices for this decoding analysis, we also showed, as expected, that low current stimuli (close to threshold) and stimuli above 1.2 mA did not generate distinguishable responses (figure 3(e)). For low current stimuli, we posit that this is due to sub-threshold responses, where no significant change in the recorded waveforms occurs when compared to pre-stimulus periods; high current stimuli would have resulted in consistent saturated responses, leading to our algorithm being unable to decode the correct stimulation parameters.

The greater ability to generate distinguishable responses in this study compared to that reported by Cottaris and Elfar (2009) may be due to a larger stimulus set being tested as well as a larger separation between stimulating electrodes (0.68° for the epi-retinal electrodes versus 4° for electrodes used in these experiments). However, the information metric does highlight the advantages of the suprachoroidal approach in targeting a wide visual field allowing for more unique, easily distinguished responses (~40).

While these analyses do not answer whether the visual system is actually taking advantage of the features used in the decoders, the information metric allows benchmark comparison of the evoked neural responses across experimental paradigms. The analyses, specifically the decoding results, also indicate that a large set of different cortical responses are being evoked through suprachoroidal stimulation and future work may help close the gap between the number of distinguishable cortical responses that can be evoked and spatially distinguishable phoshenes reported by human patients.

Acknowledgments

The authors wish to thank Felix Aplin, Patrick Atkinson, Rosemary Cicione, Sam John, and Ronald Leung for assistance with data collection, Michelle McPhedran and Alexia Saunders for technical assistance, Penelope Allen and Jonathan Yeoh who performed all surgeries, and Owen Burns, Helen Feng, and Vanessa Maxim for electrode array fabrication. We also wish to thank Rob Shepherd, Chris Williams and James Fallon for overall guidance and advice during the *in vivo* experiments. This research was supported by the Australian Research Council's Discovery Projects funding scheme (DP140104533) and through its Special Research Initiative (SRI) in Bionic Vision Science and Technology awarded to Bionic Vision Australia (BVA) SR1000005. The contribution of MNS was funded by a project grant from the National Health and Medical Research Council Australia (GNT1063093). The research was also supported by the Bertalli Family Foundation through the Bionics Institute. The Bionics Institute acknowledges the support received from the Victorian Government through its Operational Infrastructure Program. This research was supported by a Victorian Life Sciences Computation Initiative (VLSCI) grant number [VR0138] on its Peak Computing Facility at the University of Melbourne, an initiative of the Victorian Government, Australia.

References

Ayton L N *et al* 2014 First-in-human trial of a novel suprachoroidal retinal prosthesis *PLoS One* **9** e115239

Buzsáki G, Anastassiou C A and Koch C 2012 The origin of extracellular fields and currents—EEG, ECoG, LFP and spikes *Nat. Rev. Neurosci.* **13** 407–20

Buzsáki G and Schomburg E W 2015 What does gamma coherence tell us about inter-regional neural communication? *Nat. Neurosci.* **18** 484–9

Chao Z C, Nagasaka Y and Fujii N 2010 Long-term asynchronous decoding of arm motion using electrocorticographic signals in monkeys *Front. Neuroeng.* **3** 3

Cicione R, Fallon J B, Rathbone G D, Williams C E and Shivdasani M N 2014 Spatiotemporal interactions in the visual cortex following paired electrical stimulation of the retina *Invest. Ophthalmol. Vis. Sci.* **55** 7726–38

Cottaris N P and Elfar S D 2009 Assessing the efficacy of visual prostheses by decoding ms-LFPs: application to retinal implants *J. Neural Eng.* **6** 026007

Donner T H and Siegel M 2011 A framework for local cortical oscillation patterns *Trends Cogn. Sci.* **15** 191–9

Dorn J D, Ahuja A K, Caspi A, da Cruz L, Dagnelie G, Sahel J-A, Greenberg R J and McMahon M J 2013 The detection of motion by blind subjects with the Epiretinal 60-Electrode (Argus II) retinal prosthesis *JAMA Ophthalmol.* **131** 183–9

Duda R O, Hart P E and Stork D G 2012 *Pattern Classification* (New York: Wiley)

Dumm G, Fallon J B, Williams C E and Shivdasani M N 2014 Virtual electrodes by current steering in retinal prostheses *Invest. Ophthalmol. Vis. Sci.* **55** 8077–85

Eckhorn R *et al* 2006 Visual resolution with retinal implants estimated from recordings in cat visual cortex *Vis. Res.* **46** 2675–90

Flint R D, Lindberg E W, Jordan L R, Miller L E and Slutzky M W 2012 Accurate decoding of reaching movements from field potentials in the absence of spikes *J. Neural. Eng.* **9** 046006

Flint R D, Wright Z A, Scheid M R and Slutzky M W 2013 Long term, stable brain machine interface performance using local field potentials and multiunit spikes *J. Neural Eng.* **10** 056005

Fries P 2005 A mechanism for cognitive dynamics: neuronal communication through neuronal coherence *Trends Cogn. Sci.* **9** 474–80

Fujikado T *et al* 2007 Evaluation of phosphenes elicited by extraocular stimulation in normals and by suprachoroidal-transretinal stimulation in patients with retinitis pigmentosa *Graefe's Arch. Clin. Exp. Ophthalmol.* **245** 1411–9

Fujikado T *et al* 2011 Testing of semichronically implanted retinal prosthesis by suprachoroidal-transretinal stimulation in patients with retinitis pigmentosa *Invest. Ophthalmol. Vis. Sci.* **52** 4726–33

Gray C M, König P, Engel A K and Singer W 1989 Oscillatory responses in cat visual cortex exhibit inter-columnar synchronization which reflects global stimulus properties *Nature* **338** 334–7

Ho A C *et al* 2015 Long-term results from an epiretinal prosthesis to restore sight to the blind *Ophthalmology* **122** 1547–54

Hubel D H and Wiesel T N 1959 Receptive fields of single neurones in the cat's striate cortex *J. Physiol.* **148** 574–91

Humayun M S *et al* 2003 Visual perception in a blind subject with a chronic microelectronic retinal prosthesis *Visi. Res.* **43** 2573–81

Jepson L H, Hottowy P, Mathieson K, Gunning D E, Dąbrowski W, Litke A M and Chichilnisky E J 2014a Spatially patterned electrical stimulation to enhance resolution of retinal prostheses *J. Neurosci.* **34** 4871–81

Jepson L H, Hottowy P, Weiner G A, Dabrowski W, Litke A M and Chichilnisky E J 2014b High-fidelity reproduction of spatiotemporal visual signals for retinal prosthesis *Neuron* **83** 87–92

Katzner S, Nauhaus I, Benucci A, Bonin V, Ringach D L and Carandini M 2009 Local origin of field potentials in visual cortex *Neuron* **61** 35–41

Kayser C, Montemurro M A, Logothetis N K and Panzeri S 2009 Spike-phase coding boosts and stabilizes information carried by spatial and temporal spike patterns *Neuron* **61** 597–608

Kayser C, Salazar R F and Konig P 2003 Responses to natural scenes in cat V1 *J. Neurophysiol.* **90** 1910–20

Leuthardt E C, Schalk G, Wolpaw J R, Ojemann J G and Moran D W 2004 A brain–computer interface using electrocorticographic signals in humans *J. Neural. Eng.* **1** 63–71

Maris E, Schoffelen J-M and Fries P 2007 Nonparametric statistical testing of coherence differences *J. Neurosci. Methods* **163** 161–75

Markowitz D A, Wong Y T, Gray C M and Pesaran B 2011 Optimizing the decoding of movement goals from local field potentials in macaque cortex *J. Neurosci.* **31** 18412–22

Miller G 1955 Note on the bias of information estimates *Information Theory in Psychology Problems and Methods II-B* pp 95–100

Mitra P P and Pesaran B 1999 Analysis of dynamic brain imaging data *Biophys. J.* **76** 691–708

Mitzdorf U 1985 Current source-density method and application in cat cerebral cortex: investigation of evoked potentials and EEG phenomena *Physiol. Rev.* **65** 37–100

Nakauchi K *et al* 2005 Transretinal electrical stimulation by an intrascleral multichannel electrode array in rabbit eyes *Graefe's Arch. Cinical Exp. Ophthalmol.* **243** 169–74

Panzeri S, Senatore R, Montemurro M A and Petersen R S 2007 Correcting for the sampling bias problem in spike train information measures *J. Neurophysiol.* **98** 1064–72

Priori A, Foffani G, Rossi L and Marceglia S 2013 Adaptive deep brain stimulation (aDBS) controlled by local field potential oscillations *Exp. Neurol.* **245** 77–86

Ray S and Maunsell J H R 2011 Different origins of gamma rhythm and high-gamma activity in macaque visual cortex *PLoS Biol.* **9** e1000610

Sakaguchi H *et al* 2004 Transretinal electrical stimulation with a suprachoroidal multichannel electrode in rabbit eyes *Japan. J. Ophthalmol* **48** 256–61

Saunders A L *et al* 2014 Development of a surgical procedure for implantation of a prototype suprachoroidal retinal prosthesis *Clin. Exp. Ophthalmol.* **42** 665–74

Schanze T, Wilms M, Eger M, Hesse L and Eckhorn R 2002 Activation zones in cat visual cortex evoked by electrical retina stimulation *Graefe's Arch. Clin. Exp. Ophthalmol.* **240** 947–54

Schomburg E W, Anastassiou C A, Buzsáki G and Koch C 2012 The spiking component of oscillatory extracellular potentials in the rat hippocampus *J. Neurosci.* **32** 11798–811

Shivdasani M N, Sinclair N C, Dimitrov P N, Varsamidis M, Ayton L N, Luu C D, Perera T, McDermott H J and Blamey P J 2014 Factors affecting perceptual thresholds in a suprachoroidal retinal prosthesis *Invest. Ophthalmol. Vis. Sci.* **55** 6467–81

Siegel M, Donner T H and Engel A K 2012 Spectral fingerprints of large-scale neuronal interactions *Nat. Rev. Neurosci.* **13** 121–34

Stingl K *et al* 2015 Subretinal visual implant alpha IMS—clinical trial interim report *Vis. Res.* **111** 149–60

Thomson D J 1982 Spectrum estimation and harmonic analysis *Proc. IEEE* **70** 1055–96

Tusa R J, Palmer L A and Rosenquist A C 1978 The retinotopic organization of area 17 (striate cortex) in the cat *J. Comp. Neurol.* **177** 213–35

Vinck M, Lima B, Womelsdorf T, Oostenveld R, Singer W, Neuenschwander S and Fries P 2010 Gamma-phase shifting in awake monkey visual cortex *J. Neurosci.* **30** 1250–7

Waldert S, Pistohl T, Braun C, Ball T, Aertsen A and Mehring C 2009 A review on directional information in neural signals for brain-machine interfaces *J. Physiol. Paris* **103** 244–54

Walter P, Kisvárday Z F, Görtz M, Alteheld N, Rossler G, Stieglitz T and Eysel U T 2005 Cortical activation via an implanted wireless retinal prosthesis *Invest. Ophthalmol. Vis. Sci.* **46** 1780–5

Weliky M, Fiser J, Hunt R H and Wagner D N 2003 Coding of natural scenes in primary visual cortex *Neuron* **37** 703–18

Wilke R *et al* 2011 Spatial resolution and perception of patterns mediated by a subretinal 16-electrode array in patients blinded by hereditary retinal dystrophies *Invest. Ophthalmol. Vis. Sci.* **52** 5995–6003

Wilson B S and Dorman M F 2008 Cochlear implants: a remarkable past and a brilliant future *Hear. Res.* **242** 3–21

Wolpaw J R, Birbaumer N, McFarland D J, Pfurtscheller G and Vaughan T M 2002 Brain–computer interfaces for communication and control *Clin. Neurophysiol.* **113** 767–91

Wong Y T, Chen S C, Seo J M, Morley J W, Lovell N H and Suaning G J 2009 Focal activation of the feline retina via a suprachoroidal electrode array *Vis. Res.* **49** 825–33

Xing D, Yeh C-I and Shapley R M 2009 Spatial spread of the local field potential and its laminar variation in visual cortex *J. Neurosci.* **29** 11540–9

Zrenner E 2013 Fighting blindness with microelectronics *Sci. Transl. Med.* **5** 210ps16

Zrenner E *et al* 2011 Subretinal electronic chips allow blind patients to read letters and combine them to words *Proc. Biol. Sci./R. Soc.* **278** 1489–97